



This is a repository copy of *Synthesis and characterization of poly(amino acid methacrylate)-stabilized diblock copolymer nano-objects.*

White Rose Research Online URL for this paper:
<http://eprints.whiterose.ac.uk/95151/>

Version: Supplemental Material

Article:

Ladmira, V., Charlot, A., Semsarilar, M. et al. (1 more author) (2015) Synthesis and characterization of poly(amino acid methacrylate)-stabilized diblock copolymer nano-objects. *Polymer Chemistry*, 6 (10). pp. 1805-1816. ISSN 1759-9954

<https://doi.org/10.1039/c4py01556h>

Reuse

Unless indicated otherwise, fulltext items are protected by copyright with all rights reserved. The copyright exception in section 29 of the Copyright, Designs and Patents Act 1988 allows the making of a single copy solely for the purpose of non-commercial research or private study within the limits of fair dealing. The publisher or other rights-holder may allow further reproduction and re-use of this version - refer to the White Rose Research Online record for this item. Where records identify the publisher as the copyright holder, users can verify any specific terms of use on the publisher's website.

Takedown

If you consider content in White Rose Research Online to be in breach of UK law, please notify us by emailing eprints@whiterose.ac.uk including the URL of the record and the reason for the withdrawal request.



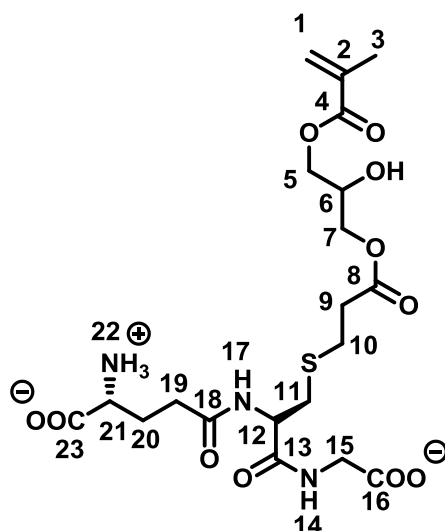
eprints@whiterose.ac.uk
<https://eprints.whiterose.ac.uk/>

Supporting Information for Polymer Chemistry manuscript:

Synthesis and characterization of poly(amino acid)-stabilized diblock copolymer nano-objects

Vincent Ladmiral,* Alexandre Charlot, Mona Semsarilar, Steven P. Armes*

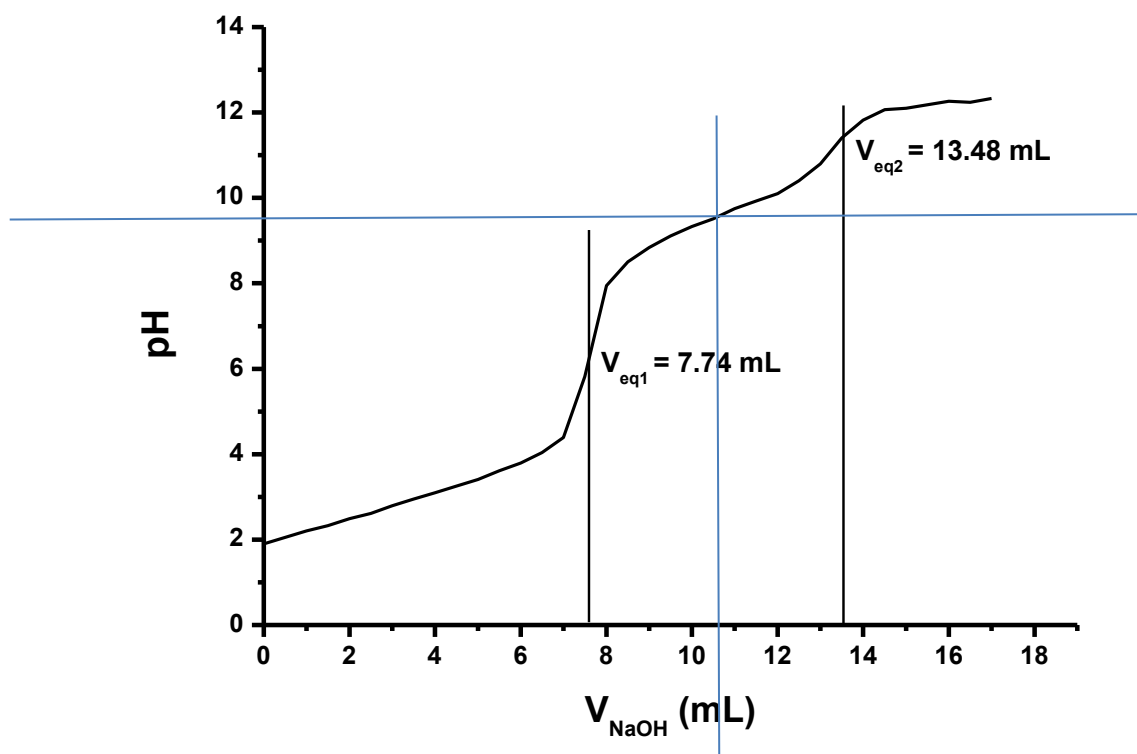
Figure S1. NMR signal assignment for GSHMA



^1H NMR (400.13 MHz, DMSO- d_6 , 298K): δ 1.95 (s, 3H₃), 2.15 (dd, 2H₁₉), 2.50-2.54 (dt, 2H₂₀), 2.74-2.89 (m, 2H₉, 2H₁₀, 2H₁₁), 3.06-3.11 (dd, 1H₁₂), 3.34 (t, 1H, OH), 3.71-3.80 (m, 4H, 1H₆, 2H₁₅, 1H₂₁), 4.20-4.25 (m, 4H, 2H₅, 2H₇), 5.77 (d, 1H_{1'}), 6.18 (d, 1H₁), 8.19 (t, 1H₁₄), 8.52 (d, 3H₂₂).

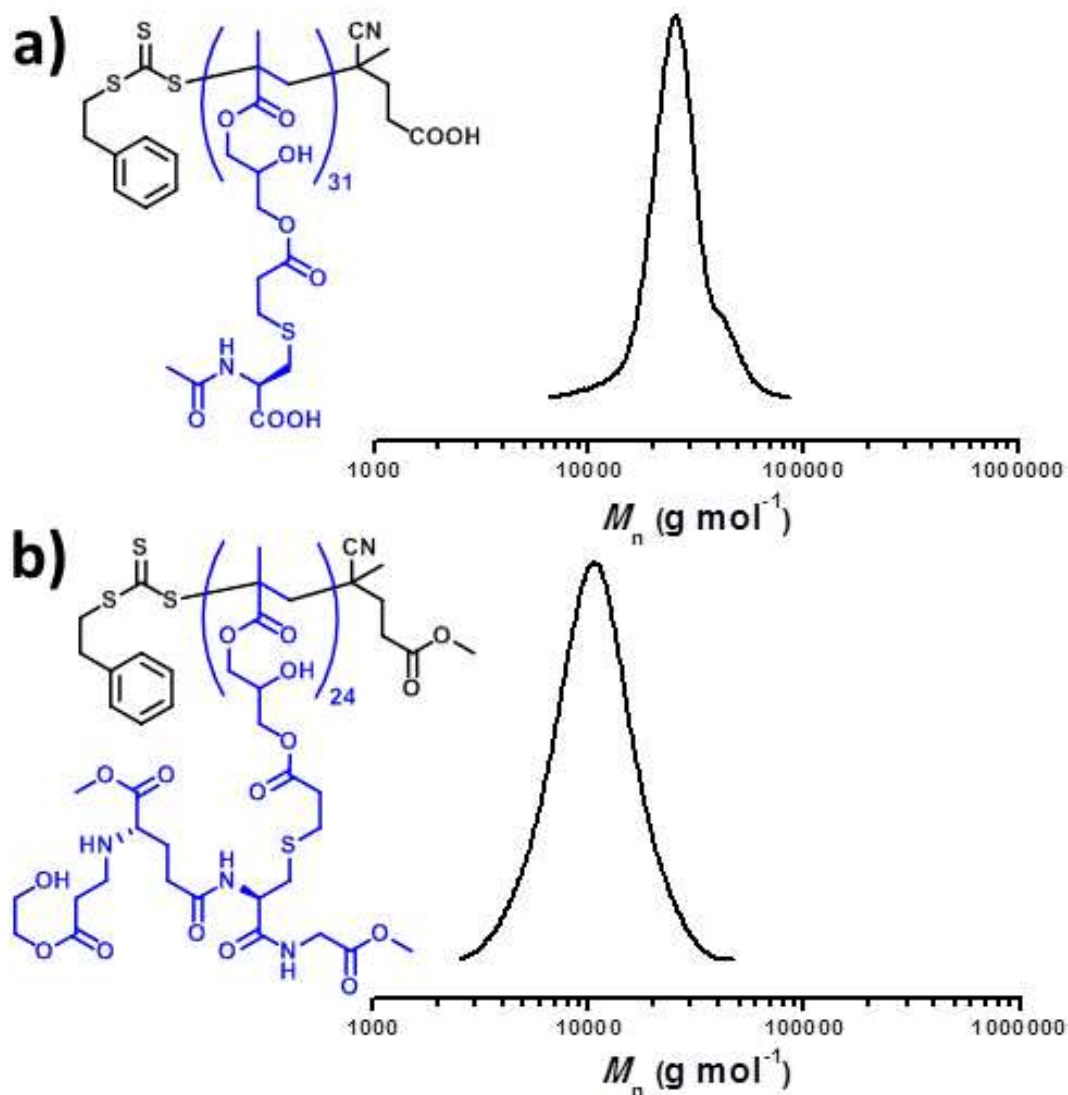
^{13}C NMR (400.13 MHz, DMSO- d_6 , 298K): δ 17.5 (C₃), 26.3 (C₂₀), 26.7 (C₁₀), 31.5 (C₁₉), 33.0 (C₁₁), 34.2 (C₉), 43.5 (C₁₅), 54.2 (C₆), 62.1 (C₂₁), 65.3 (2C, C₅, C₇), 66.9 (C₁₂), 127.3 (C₁), 135.6 (C₂), 169.3, 171.8, 174.0, 174.8, 176.1, 177.1 (6C, C₄, C₈, C₁₃, C₁₆, C₁₈, C₂₃).

Figure S2. Acid titration of glutathione methacrylate (GSHMA)



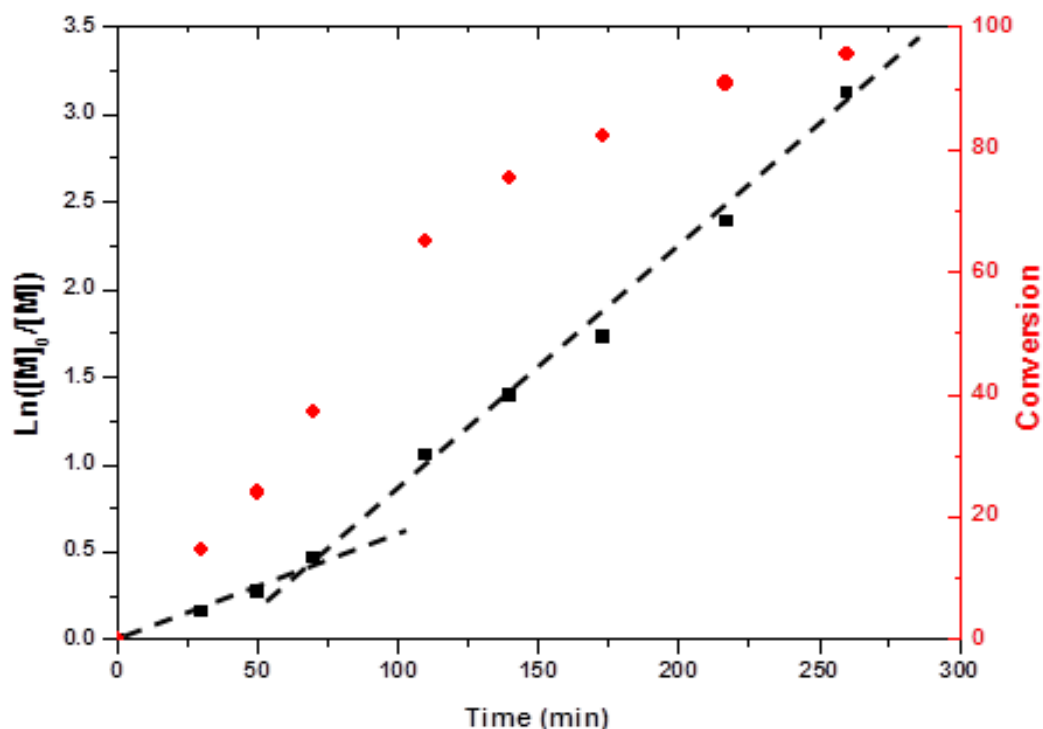
$V_0 = 1$ mL of GSHMA solution was diluted to 5 mL with DI water and titrated with an aqueous 75 mM NaOH solution. $[\text{GSHMA}]_0 = ((V_{\text{eq2}} - V_{\text{eq1}}) * C_{\text{NaOH}}) / V_0 = 0.438$ M.

Figure S3. DMF GPC chromatograms obtained for PCysMA₃₁ and PGSHMA₂₄

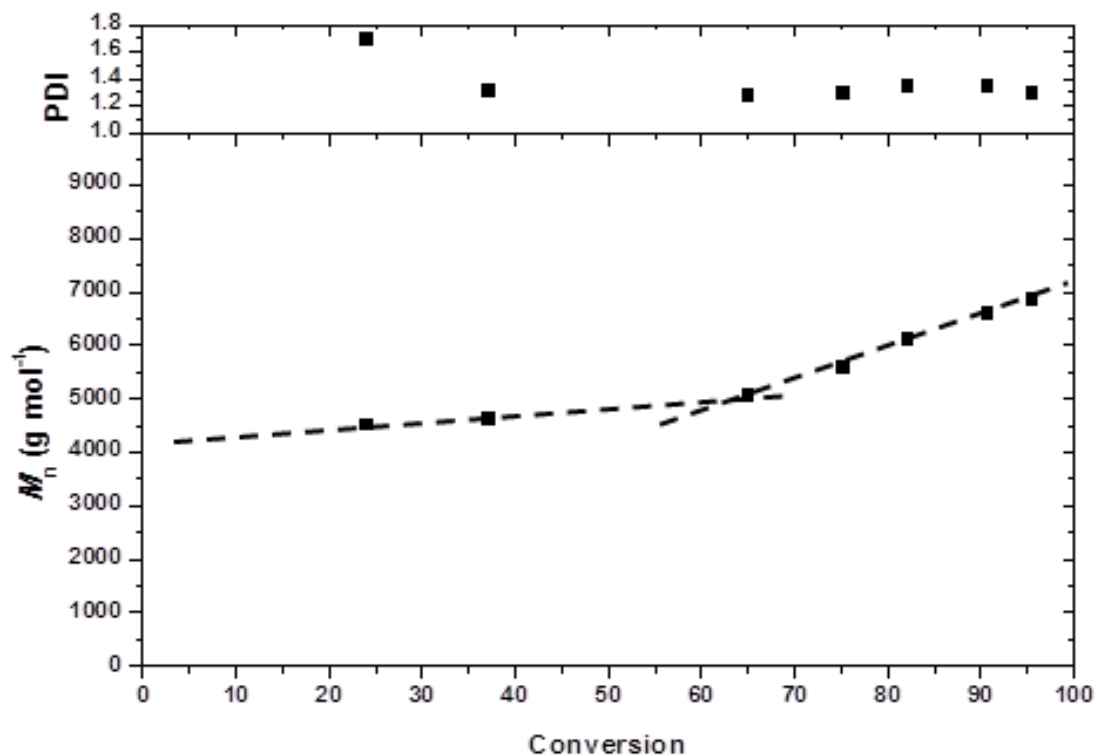


DMF gel permeation chromatograms recorded for: (a) PCysMA₃₁, 94 % conversion, M_n (NMR) = 10,700 g mol^{-1} , $M_w/M_n = 1.11$; (b) PGSHMA₂₄, 98 % conversion, M_n (NMR) = 12,800 g mol^{-1} , $M_w/M_n = 1.20$. PCysMA₃₁ and PGSHMA₂₄ were derivatized (acetylation using acetic anhydride for PCysMA₃₁ and both Michael addition with 2-hydroxyethyl acrylate and methylation with trimethylsilyl diazomethane in the case of PGSHMA₂₄) prior to GPC analysis.

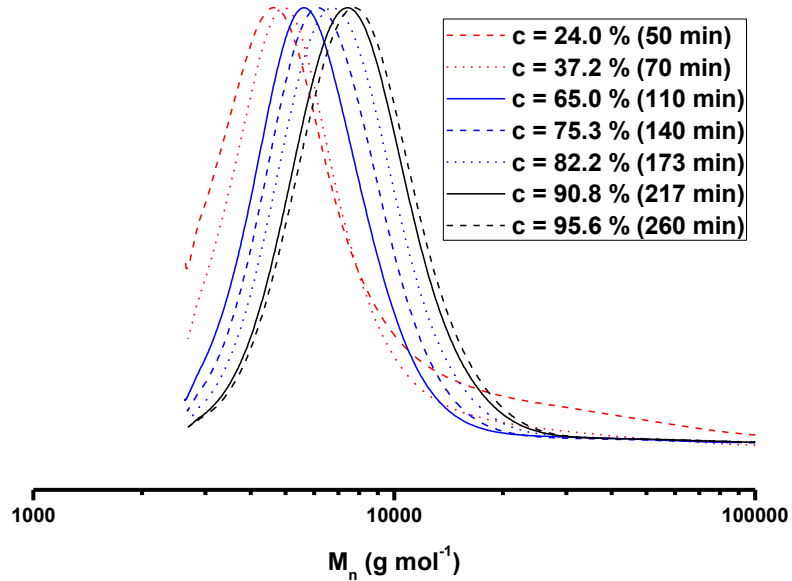
Figure S4. RAFT solution polymerization of cysteine methacrylate (CysMA)



First-order kinetic plot and evolution of conversion vs time for the RAFT polymerization of CysMA in an 83:17 w/w water/dioxane mixture at 70 °C. Reaction conditions: [CysMA] : [PETTC] : [ACVA] = 50 : 1 : 0.2, [CysMA] = 9 wt %.

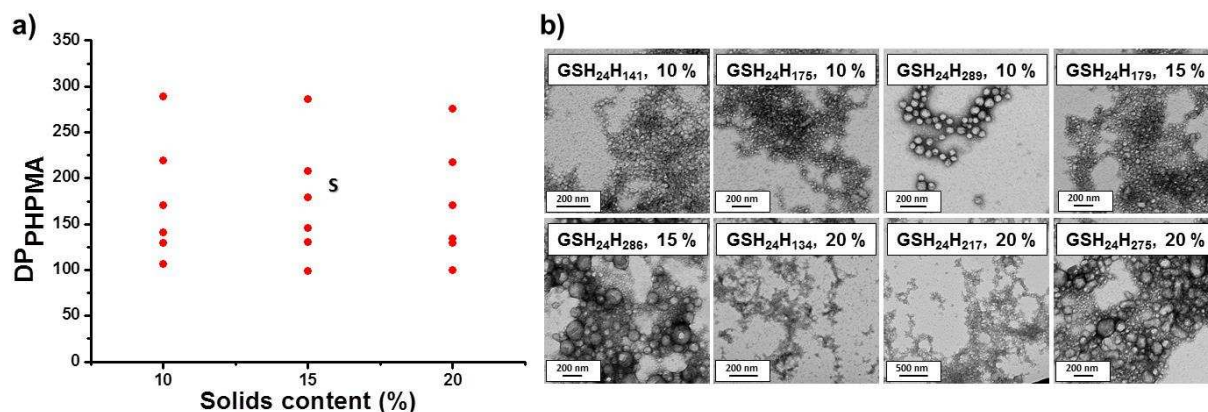


Evolution of M_n and polydispersity vs conversion for the RAFT polymerization of CysMA in an 83:17 w/w water/dioxane mixture at 70 °C. Reaction conditions: [CysMA] : [PETTC] : [ACVA] = 50 : 1 : 0.2, [CysMA] = 9 wt %.



Aqueous GPC chromatograms obtained for samples taken at different times during the RAFT solution polymerization of CysMA in water/dioxane mixture.

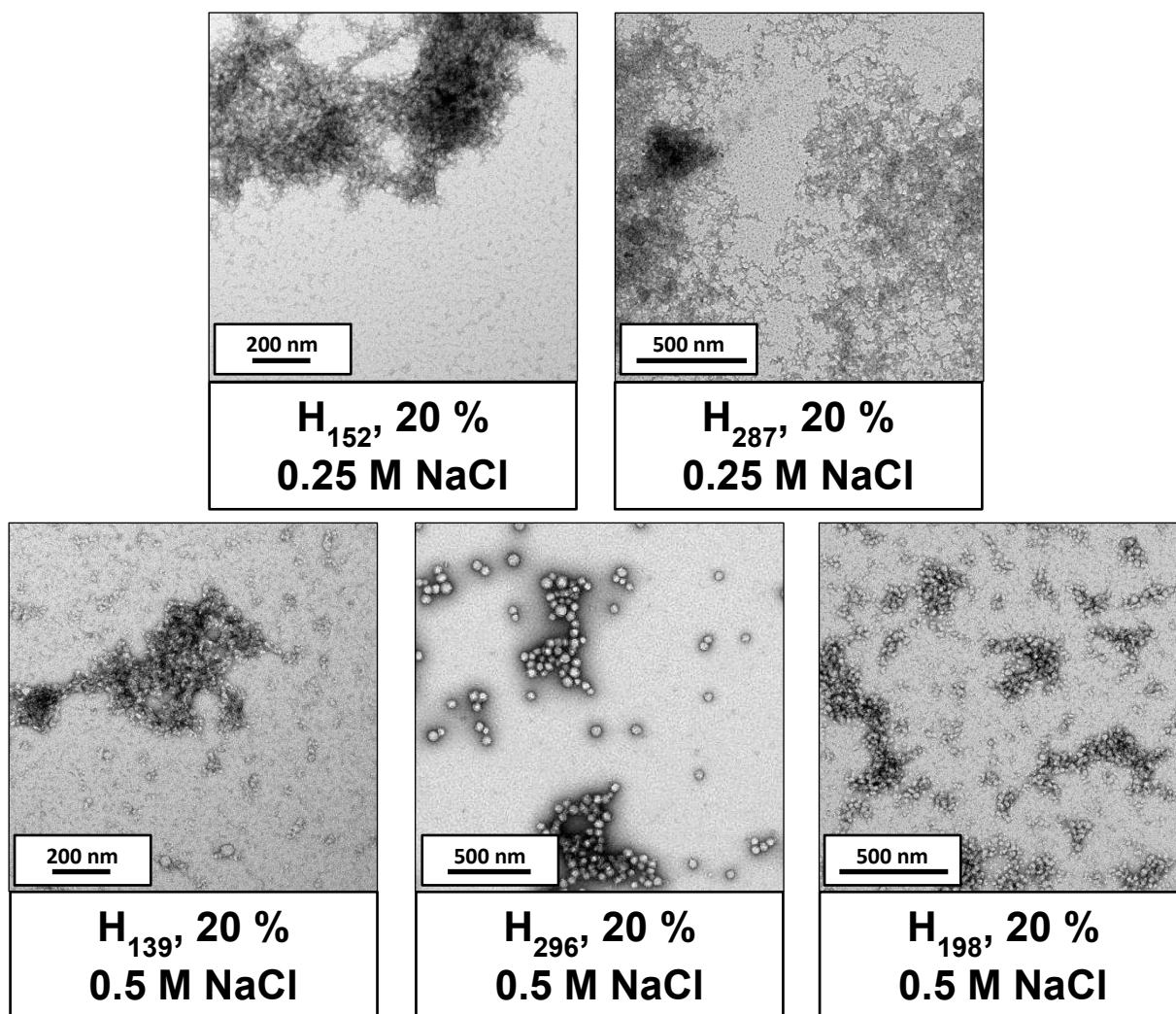
Figure S5. Phase diagram and representative TEM images obtained for the RAFT aqueous dispersion polymerization of HPMA using a PGSHMA₂₄ macro-CTA



(a) Phase diagram constructed for PGSHMA₂₄–PHPMA_x diblock copolymer nano-objects prepared by RAFT aqueous dispersion polymerization of HPMA using a PGSHMA₂₄ macro-CTA at 70 °C. The target PHPMA DP and the total solids content were systematically varied and the *post mortem* copolymer morphologies obtained at > 98 % HPMA conversion were determined by TEM. N.B. S denotes spheres.

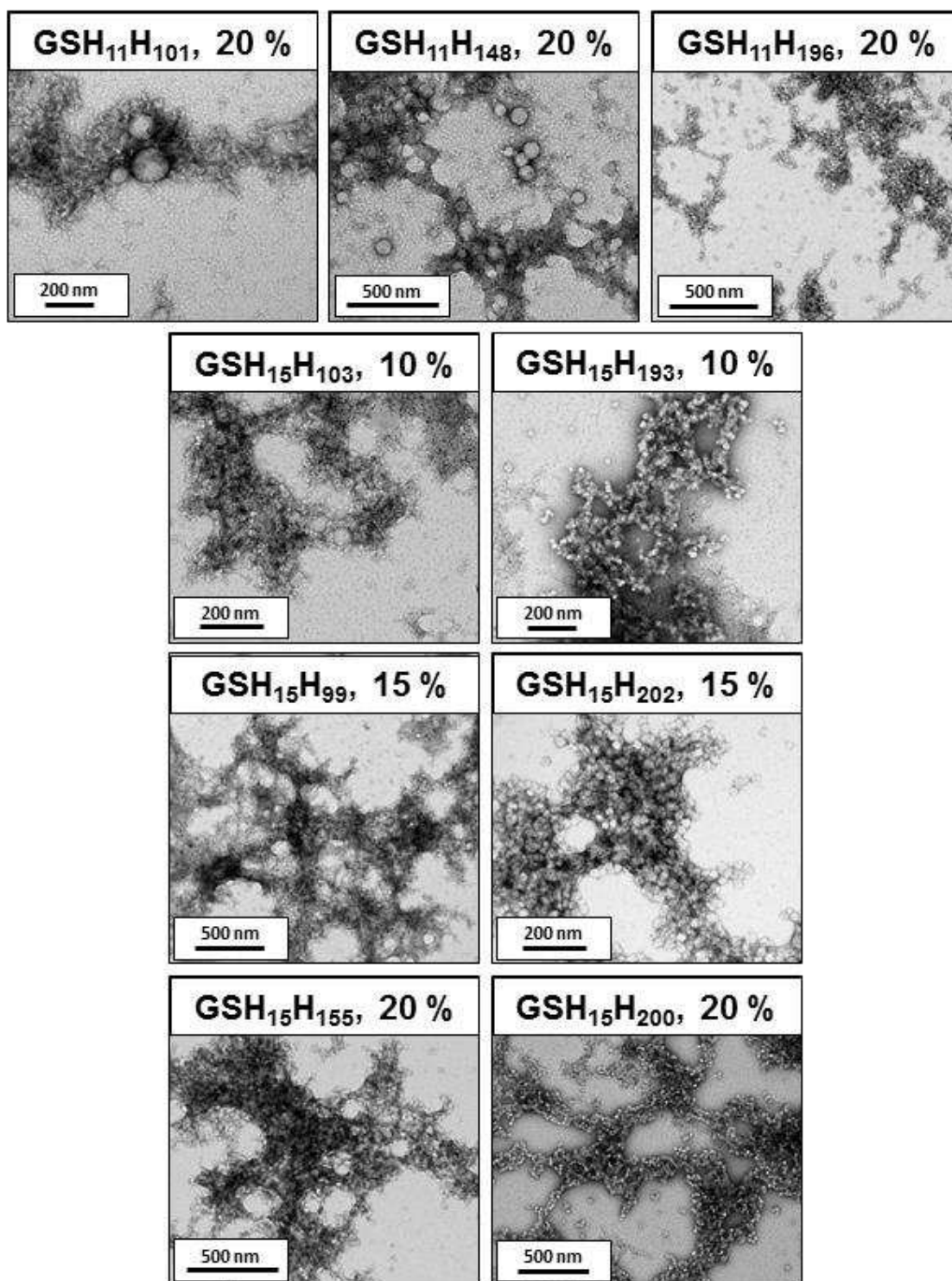
(b) Representative TEM images obtained for PGSHMA₂₄–PHPMA_x (denoted GSH₂₄–H_x for brevity) diblock copolymer nano-objects prepared by RAFT aqueous dispersion polymerization of HPMA at 70 °C. The target block composition and copolymer solids content % are indicated on each image.

Figure S6. TEM images obtained for diblock copolymer nano-objects formed in the presence of NaCl



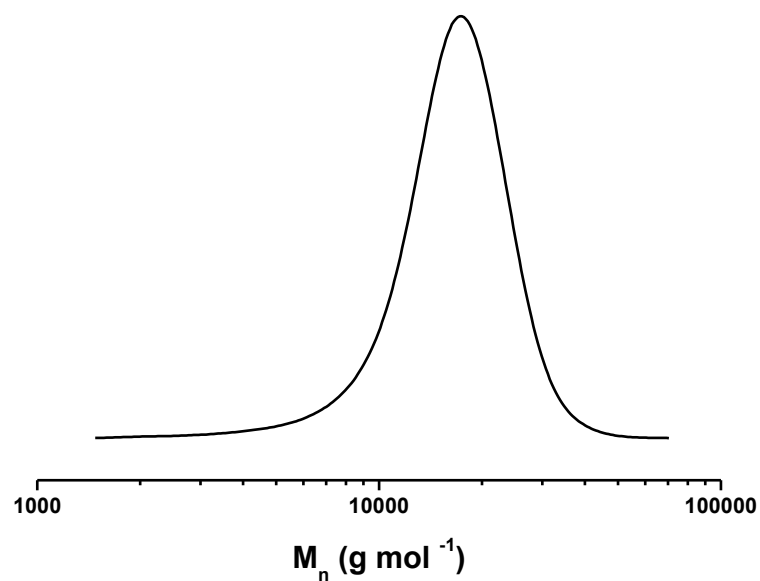
Representative TEM images obtained for PGSHMA₂₄-PHPMA_x diblock copolymer nano-objects prepared by RAFT aqueous dispersion polymerization of HPMA at 70 °C in the presence of NaCl. The targeted DP for the PHPMA block (herein denoted by 'H' for brevity) and the copolymer solids content % is indicated on each image.

Figure S7. TEM images obtained for diblock copolymer nano-objects prepared using relatively short PGSHMA macro-CTAs



Representative TEM images obtained for $\text{PGSHMA}_{11}\text{-PHPMA}_x$ and $\text{PGSHMA}_{15}\text{-PHPMA}_x$ diblock copolymer nano-objects prepared by RAFT aqueous dispersion polymerization of HPMA at 70 °C. The targeted DP for the PHPMA block (herein denoted by 'H' for brevity) and the copolymer solids content % is indicated on each image.

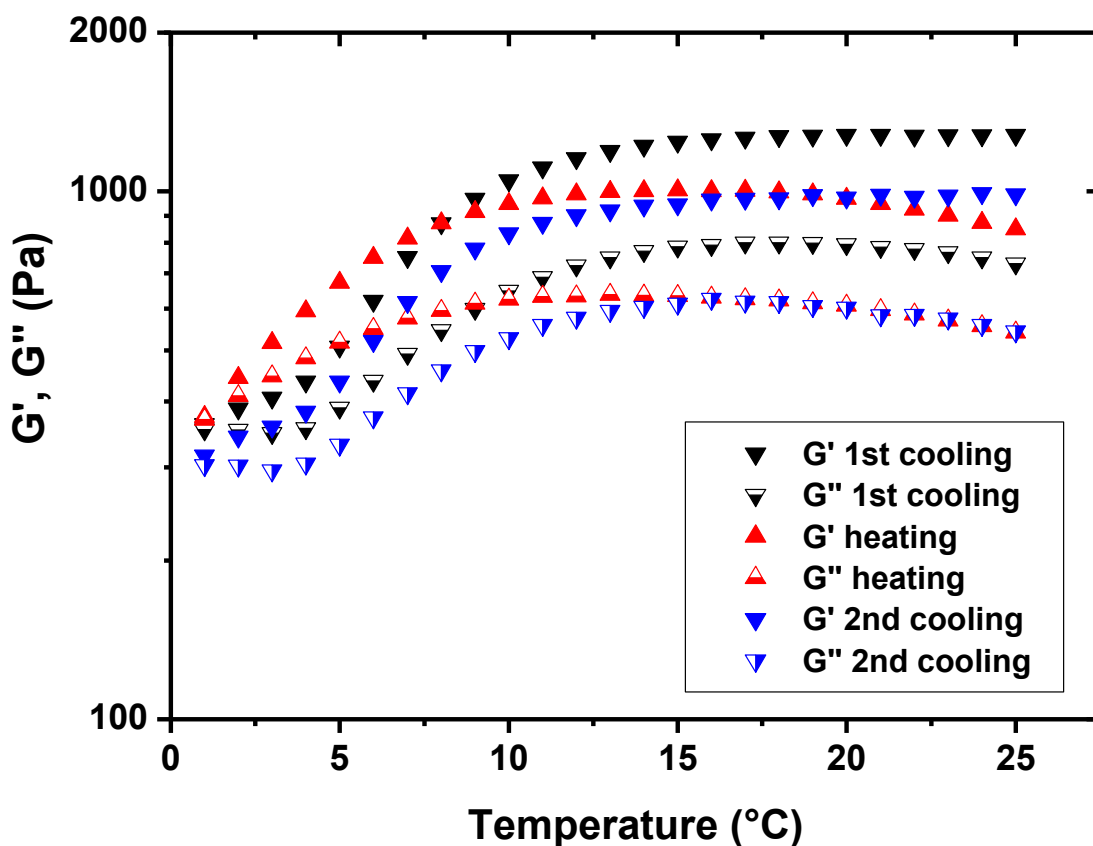
Figure S8. DMF GPC chromatogram obtained for PGMA₅₅ macro-CTA



DMF GPC chromatogram obtained for PGMA₅₅ :

$M_n = 15,100 \text{ g mol}^{-1}$, $M_w = 19,600 \text{ g mol}^{-1}$, $M_w / M_n = 1.15$

Figure S9. Temperature dependence of the storage and loss moduli observed for a 20 % w/w PGSHMA₂₄ + PGMA₅₅)-PHPMA₁₇₈ diblock copolymer worm gel dispersion

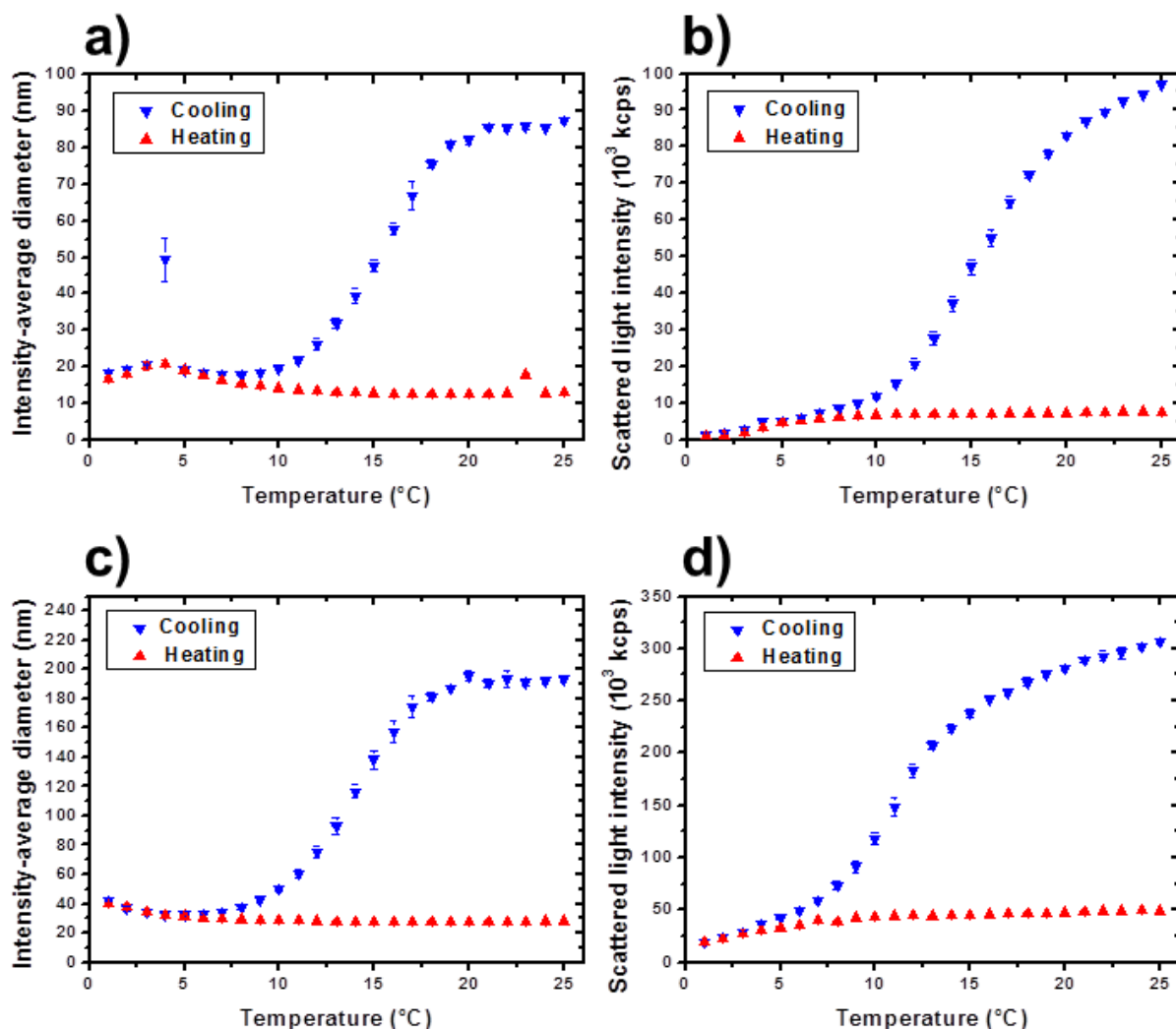


Variation of storage modulus (G') and loss modulus (G'') for a 20% w/w (1:9 PGSHMA₂₄ + PGMA₅₅)-PHPMA₁₇₈ diblock copolymer worm gel dispersion during the following temperature cycling: (i) cooling from 25 to 1 °C (G' = inverted black triangles, G'' = inverted black and white triangles); (ii) subsequent warming from 1 to 25 °C in 1 °C increments (G' = red triangles, G'' = red and white triangles) and (iii) cooling from 25 to 1 °C in 1 °C increments (G' = inverted blue triangles, G'' = inverted blue and white triangles).

Notes: The cross-over temperature appeared to be slightly below 1 °C in this case.

Hysteresis is observed between the first cooling and heating cycles. This was much less marked between the heating and the second cooling cycles.

Figure S10. Temperature-dependent DLS studies of diblock copolymer worm dispersions

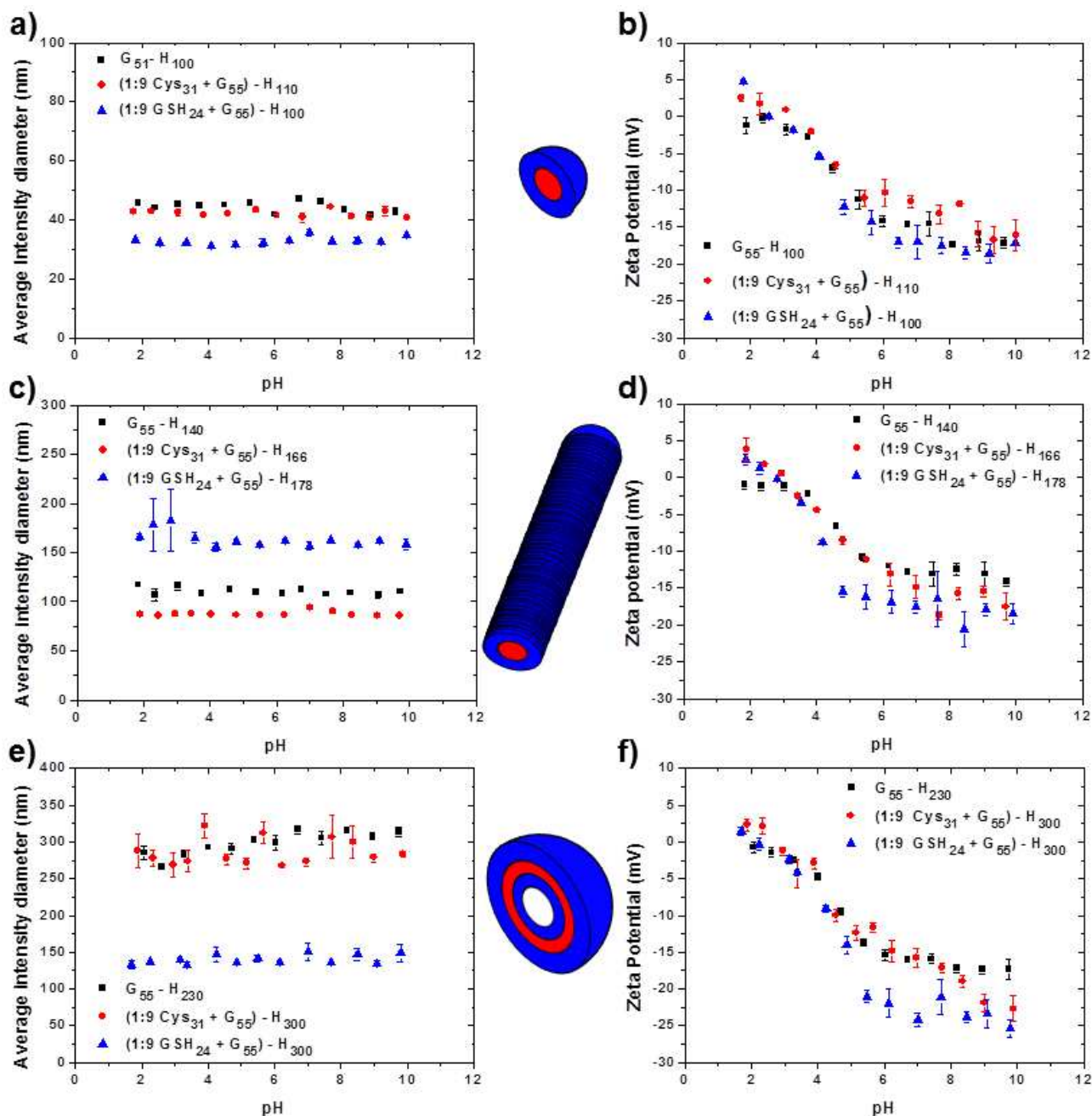


Temperature-dependent DLS studies, showing the variation in intensity-average diameter and scattered light intensity respectively, for: (a, b) a (1:9 PCysMA₃₁ + PGMA₅₅)-PHPMA₁₆₆ dispersion of diblock copolymer worms diluted to 1% w/w; (c, d) a (1:9 PGSHMA₂₄ + PGMA₅₅)-PHPMA₁₇₈ dispersion of diblock copolymer worms diluted to 1.0% w/w.

In the case of (1:9 PCysMA₃₁ + PGMA₅₅)-PHPMA₁₆₆ (see Figures S10a and S10b), the apparent sphere-equivalent hydrodynamic diameter decreases from around 90 nm at 25°C to 20 nm at 1°C, with a concomitant reduction in the scattered light intensity. These measurements are consistent with visual observations and rheological data and confirm that degelation occurs via a worm-to-sphere transition. However, on warming the cold 1% w/w copolymer dispersion to ambient temperature, the sphere-to-worm transition is *not* observed, even on standing for relatively long time scales (weeks). This is because of the reduced probability of efficient 1D fusion of spheres at this relatively low copolymer concentration.^{76b}

The DLS data (see Figures S11c and S11d) are very similar to those obtained for a dilute dispersion of (1:9 PCysMA₃₁ + PGMA₅₅)-PHPMA₁₆₆. Thus cooling a 1% w/w dispersion of (1:9 PGSHMA₂₄ + PGMA₅₅)-PHPMA₁₇₈ diblock copolymer nano-objects results in a near-monotonic reduction in particle size and scattered light intensity. Polydisperse worms with a sphere-equivalent diameter of 180 nm were observed at 25°C, while near-monodisperse spheres of 40 nm were obtained below 10°C. No sphere-to-worm transition occurred on returning to 25°C, confirming that the (ir)reversibility of this thermal transition has a strong concentration dependence.

Figure S11. Variation of zeta potential and intensity-average diameter with pH for spheres, worms and vesicles.



Variation of zeta potential and intensity-average diameter with pH for spheres, worms and vesicles. (a) Intensity-average diameter vs. pH for $\text{PGMA}_{55}\text{-PHPMA}_{100}$ spheres (black squares), $(1:9 \text{ PCysMA}_{31} + \text{PGMA}_{55})\text{-PHPMA}_{110}$ (red circles), and $(1:9 \text{ PGSHMA}_{24} + 0.9\text{PGMA}_{55})\text{-PHPMA}_{100}$ (blue triangles). (b) Zeta potential vs. pH for the same diblock copolymer dispersions. (c) Intensity-average diameter vs pH for $\text{PGMA}_{55}\text{-PHPMA}_{140}$ worms (black squares), $(1:9 \text{ PCysMA}_{31} + \text{PGMA}_{55})\text{-PHPMA}_{166}$ (red circles), and $(1:9 \text{ PGSHMA}_{24} + \text{PGMA}_{55})\text{-PHPMA}_{178}$ (blue triangles). (d) Zeta potential vs. pH for the same diblock copolymer dispersions. (e) Intensity diameter vs pH for $\text{PGMA}_{55}\text{-PHPMA}_{230}$ vesicles (black squares), $(1:9 \text{ PCysMA}_{31} + \text{PGMA}_{55})\text{-PHPMA}_{300}$ (red circles), and $(1:9 \text{ PGSHMA}_{24} + \text{PGMA}_{55})\text{-PHPMA}_{300}$ (blue triangles). (f) Zeta potential vs. pH for the same diblock copolymer dispersions.